International Journal of Fracture **82:** 381–399, 1996.

Analysis of a crack in a disclinated cylinder

MAO S. WU and HONG ZHOU
Department of Engineering Mechanics, University of Nebraska–Lincoln, 212 Bancroft Hall, Lincoln, NE 68588-0347, USA

Received 10 September 1996; accepted in revised form 6 December 1996

Abstract. In this paper, the stress intensity factors and the opening displacement of a crack loaded by a negative wedge disclination in an isotropic cylinder are numerically determined. The disclination axis coincides with the long axis of the cylinder, and one end of the crack coincides with the disclination location. The cylinder may also be subjected to equal and opposite line loads on its surface. An exact formulation leads to a pair of decoupled singular integral equations of the Cauchy type. Numerical solutions show that if the cylinder represents a grain in a polycrystal, (i) unstable submicroscopic cracks 10^{-5} to 10^{-1} times the grain size and stable microscopic cracks of the order of the grain size, are predicted, (ii) the submicroscopic crack length to grain size ratio decreases, while the microscopic crack length to grain size ratio increases, as the grain size increases, (iii) significant differences exist, even in the case of the submicroscopic cracks, between the predictions of the exact theory and the approximate theory which ignores stress redistribution, and (iv) the opening displacement is independent of the elastic constants and the crack profile is wedge-shaped.

Key words: disclinations, submicroscopic and microscopic cracks, stress intensity factors, opening displacements

1. Introduction

Disclinations exist as rotational defects in polycrystalline aggregates. Bollman [1, 2] described the mathematical structure of a triple line disclination. This description rests on the interpretation of grain boundaries as dislocation networks. Typically, three such networks meet at the triple line. The dislocation balance between the networks at the triple line, however, may or may not be satisfied. If it is satisfied, the triple line is called an I-line. If it is not satisfied, then the triple line acquires the character of a disclination and is called a U-line.

Geometrically, disclinations are elementary carriers of rotations and can be used to describe the rotational deformation of plastic flow. This view is based on experimental observations of the rotation of microregions during the plastic deformation of polycrystals. The rotational modes of plasticity become increasingly important while the translational modes decrease in importance as the strain exceeds ~ 0.4. The rotations can produce a fragmented structure consisting of strongly misoriented microregions. Romanov and Vladimirov [3] provided an extensive review of both the theoretical and experimental aspects of the subject, including a comprehensive list of literature. In particular, consideration of the geometry of a straight disclination leads to its classification as either a twist or a wedge disclination. If the Frank vector of a disclination is perpendicular to the defect line, the disclination is twist. If the Frank vector is parallel to the defect line, the disclination is wedge.

The analysis of disclinations and their effect on polycrystalline deformation continues to attract attention. For instance, Belov [4] investigated the stress field of a wedge disclination in an anisotropic rotationally inhomogeneous medium. Nazarov, Romanov and Valiev [5] studied the stress field and the energy of nonequilibrium grain boundaries in which disclinations in triple lines constitute an important component. Also, Nazarov [6] investigated the effect of

a disclination dipole on the grain size dependence of the flow stress as described by the Hall-Petch relation.

A disclination possesses a singular stress field and is a source of large internal stresses. The power of a disclination in a polycrystal typically lies between 0.1° and 5° [3]. Powers greater than 10° are considered large. A crack can nucleate under the internal stresses. Rybin and Zhukovskii [7] investigated the nucleation of a crack due to the formation of a wedge disclination loop at the triple line of fragments or grains. For a disclination of power equal to $-1.72°$, a fragment size of 0.5 μm, an effective surface energy of 1 J/m^2, and a theoretical tensile strength equal to $\mu/30$ (μ is the shear modulus), they predicted the crack size to be approximately 0.07 μm. This prediction is consistent with experimental data (e.g., Lyles and Wilsdorf [8], Regel, Leksovskii and Sakiev [9]). Furthermore, experimental observations reveal that the nucleated cracks are often wedge-shaped [7]. More recently, Gutkin and Ovid'ko [10] suggested that a triple line disclination can split into disclinations of smaller powers. The splitting is associated with the local amorphization of the triple lines and competes with microcrack generation at the triple lines. Based on a disclination power of $-1.72°$, a structural size of 100 μm, and other parameter values similar to those of [7], they estimated that a crack nucleated from an unsplit triple line disclination is approximately 0.067 μm long. The ratio of the crack size to the structural size is 0.14 in the calculations of [7], while it is 6.7×10^{-4} according to [10]. In a recent work on crack nucleation at a disclinated triple line, Wu [11] theoretically predicted the existence of both submicroscopic cracks (subgrain size) and microscopic cracks (of the order of the grain size).

The objective of the previously mentioned works is to provide an estimate of the crack length. The redistribution of the stresses as the crack grows is ignored. The question remains, however, if it is possible to obtain a more accurate estimate. Moreover, even the accuracy of the order of the results might be in question. Second, the stability of the equilibrium crack is not investigated in [7] and [10]. Nor is the possibility of multiple crack lengths. Although these issues are considered in [11], the stress redistribution is neglected. Third, the effect of an external load is not considered. Since disclinations can be associated with internal transformations induced by external loads, consideration of external loads is of practical relevance. Fourth, the stress field used in the previous calculations is that of a disclination in a finite cylinder, whereas the Green's function formula used to compute the stress intensity factor (SIF) is appropriate for an infinite medium. Finally, the shape of the cracks has not been theoretically predicted, although experiments suggest that they are wedge-shaped as mentioned above. It is useful to predict not only qualitatively the general shape but also quantitatively the crack opening displacement, since the latter may serve as an alternative fracture parameter to the stress intensity factor.

The main objective of this paper is to compute the SIF and the opening displacement of a crack in a finite isotropic homogeneous cylinder containing a negative wedge disclination. The disclination axis coincides with the long axis of cylinder. Equal and opposite line loads may also be applied on the cylindrical surface. The five points mentioned above, i.e., stress redistribution, multiple crack length solutions and stability, the effect of an external load, the problem of a crack in a finite cylinder, and the crack opening displacement, will be explicitly considered. The method of crack analysis is based on well-known techniques, i.e., the modeling of the nucleated crack by initially unknown continuous distributions of infinitesinal edge dislocations. It requires prior knowledge of three component stress fields in an uncracked finite isotropic cylinder: the stress field of a central wedge disclination, the stress field of an off-center edge dislocation of arbitrary orientation, and the stress field due

to surface line loads. The theoretical formulation is exact, but the solutions are approximate due to the use of numerical methods.

This paper is organized in the following manner. First, the theoretical formulation is presented in Section 2. The solution technique is also described in this section. Numerical results are then provided and explained in Section 3. Finally, a list of conclusions is given in Section 4.

2. Theoretical formulation and solution

2.1. Problem description and boundary conditions

Figure 1(a) shows a negative wedge disclination of power Ω in an isotropic homogeneous cylinder of radius R. The disclination axis coincides with the long axis of the cylinder. Rectangular coordinates (x, y) and polar coordinates (r, θ) are defined with respect to the origin which is located at the center of a cross-section of the cylinder. The shear modulus and the Poisson's ratio of the cylinder are denoted respectively by μ and v. The disclination strength may then be defined as

$$D^{\nabla} = \frac{\mu\Omega}{2\pi(1-v)}, \tag{1}$$

where the superscript symbol ∇ indicates disclination. A crack of length l lies on the x-axis. The head of the crack lies at the location of the disclination where $x = 0, y = 0$. A pair of equal and opposite line loads P may also be applied to the surface of the cylinder along the y-axis.

Two sets of boundary conditions must be satisfied in this problem. First, the outer surface of the cylinder, except where the line loads are applied, must be traction-free so that the radial and shear stresses at $r = R$ must be zero, i.e.,

$$\sigma_{rr}(R, \theta) = 0, \qquad \sigma_{r\theta}(R, \theta) = 0. \tag{2}$$

Furthermore, the stress field around a negative wedge disclination is predominantly tensile and the crack is traction-free. Then, the normal and shear stresses at the location of the crack must be zero, i.e.,

$$\sigma_{yy}(x, 0) = 0, \qquad \sigma_{xy}(x, 0) = 0, \quad (0 \leqslant x \leqslant l). \tag{3}$$

2.2. Solution by superposition

To solve for the SIFs, the crack in the original problem, Figure 1(a), is replaced by an initially unknown distribution of infinitesimal edge dislocations, Figure 1(b). Then, the problem is decomposed into three subproblems, Figures 1(c), 1(d) and 1(e). In Subproblem 1, the cylinder is subjected to the internal stress field of the isolated disclination. In Subproblem 2, the cylinder is subjected to the internal loading of the dislocation distribution. In Subproblem 3, the cylinder is stressed by the equal and opposite line loads. Each subproblem is set up in such a way that (2) is automatically satisfied. The traction-free condition of (3) leads to a pair of integral equations with the dislocation distribution as unknown. To obtain these integral equations, the stress fields in all the subproblems must be known in terms of Ω, P and the dislocation

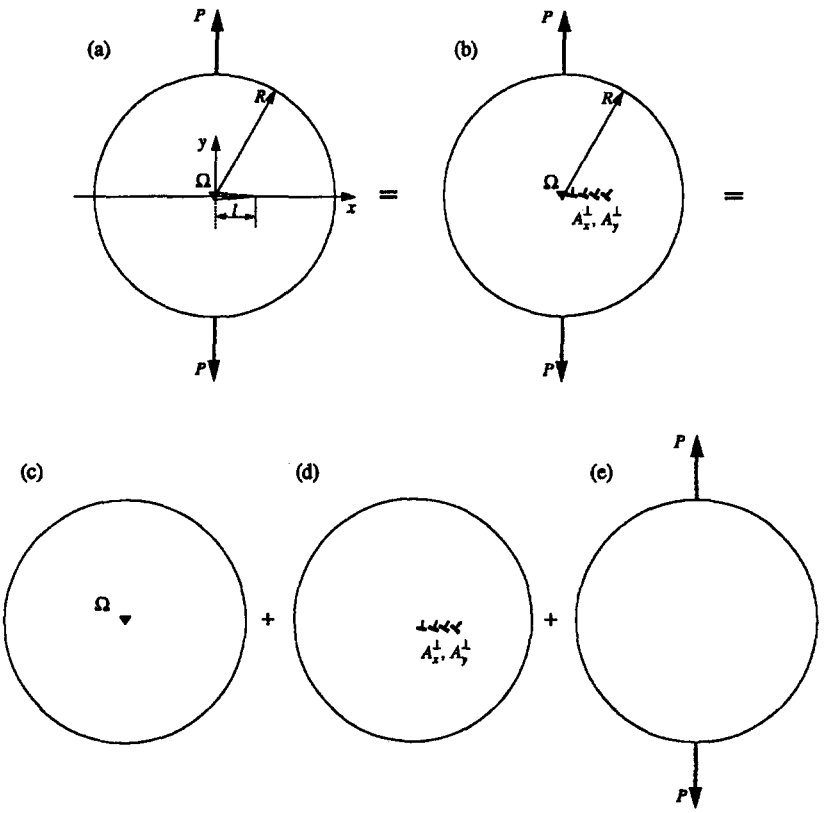

Figure 1. The decomposition of the original problem into subproblems. (a) Original problem of a crack in a disclinated cylinder. (b) Replacement of the crack by a distribution of edge dislocations. (c) Subproblem 1: the cylinder contains the singular disclination at the center. (d) Subproblem 2: the cylinder contains the distribution of edge dislocations at the original crack location. (e) Subproblem 3: the cylinder is subjected to a pair of equal and opposite surface line loads.

distribution. It is noted that the theory involving superposition is exact in the sense that all the boundary conditions are satisfied properly and any stress redistribution due to crack growth is taken into account intrinsically. If the stress redistribution is not taken into account, the theory will be called approximate in this paper.

2.3. STRESS FIELDS IN SUBPROBLEMS

In Subproblem 1, the Airy stress function and the corresponding stress field for a singular wedge disclination lying along the long axis of a cylinder are well-known (see, e.g., [3]). The Airy stress function is given by

$$\chi^{\nabla} = \tfrac{1}{2}D^{\nabla}(x^2+y^2)\left[\ln\left(\frac{\sqrt{x^2+y^2}}{R}\right) - \tfrac{1}{2}\right]. \tag{4}$$

From (4), it can be shown that the normal and shear stress components on $y = 0$ are

$$\sigma^{\nabla}_{yy}(x,0) = D^{\nabla}\left(1+\ln\frac{x}{R}\right), \tag{5}$$

$$\sigma_{xy}^{\nabla}(x,0) = 0. \tag{6}$$

Equation (5) shows that σ_{yy}^{∇} contains a logarithmic singularity. Also, σ_{yy}^{∇} changes sign at $x = R/e$, where e is the exponential. For a negative wedge disclination in which D^{∇} is negative, the transition is from a normal tensile stress to a normal compressive stress as x increases past R/e.

In Subproblem 2, the stress field in the cylinder due to an isolated edge dislocation at the eccentric location $(x, y) = (\xi_2, 0)$ can be derived from the Airy stress functions $\chi_x^{\perp}$ and $\chi_y^{\perp}$ given by Eshelby [12]. The superscript symbol $\perp$ indicates edge dislocation. Denoting the dislocation strength in the x- and y-direction as

$$D_x^{\perp} = \frac{\mu[u_x]}{2\pi(1-v)}, \qquad D_y^{\perp} = \frac{\mu[u_y]}{2\pi(1-v)}, \tag{7}$$

where $[u_x]$ and $[u_y]$ are the scalar x- and y- components of the Burgers vector of the dislocation, the Airy stress functions can be written as

$$\chi_x^{\perp} = -D_x^{\perp} y \ln\left(\frac{r^2}{r_1}\right) + D_x^{\perp}(\xi_1 - \xi_2)\frac{\xi_1}{\xi_2}\left[x - \left(\frac{\xi_1 + \xi_2}{2}\right)\right]\frac{y}{r_1^2}, \tag{8}$$

$$\chi_y^{\perp} = D_y^{\perp}(x - \xi_2)\ln\left(\frac{r_2 R}{r_1 \xi_2}\right) + \tfrac{1}{2}D_y^{\perp}(r^2 - R^2)(\xi_1 - \xi_2)\left[\frac{x - \xi_1}{\xi_2 r_1^2} + \frac{1}{R^2}\right]. \tag{9}$$

In (8) and (9), the variables ξ_1, r and $r_n, n = 1, 2$ are given by

$$\xi_1\xi_2 = R^2, \qquad r^2 = x^2 + y^2, \qquad r_n^2 = (x - \xi_n)^2 + y^2. \tag{10}$$

The normal and shear stress components on $y = 0$ are then obtained by differentiation, i.e.,

$$\begin{aligned}\sigma_{yy}^{\perp}(x,0;\xi_2) &= \left.\frac{\partial^2(\chi_x^{\perp} + \chi_y^{\perp})}{\partial x^2}\right|_{y=0} \\ &= D_y^{\perp}\left[\frac{1}{x - \xi_2} - \frac{x - 2\xi_1 + \xi_2}{(x - \xi_1)^2} + (\xi_1 - \xi_2)\right. \\ &\qquad \left.\times\left(\frac{r^2 - R^2}{\xi_2(x - \xi_1)^3} - \frac{x + \xi_1}{\xi_2(x - \xi_1)^2} + \frac{1}{R^2}\right)\right],\end{aligned} \tag{11}$$

$$\begin{aligned}\sigma_{xy}^{\perp}(x,0;\xi_2) &= -\left.\frac{\partial^2(\chi_x^{\perp} + \chi_y^{\perp})}{\partial x \partial y}\right|_{y=0} \\ &= D_x^{\perp}\left[\frac{1}{x - \xi_2} - \frac{1}{x - \xi_1} - (\xi_1 - \xi_2)\right. \\ &\qquad \left.\times\frac{\xi_1}{\xi_2}\left(\frac{1}{(x - \xi_1)^2} - \frac{2x - \xi_1 - \xi_2}{(x - \xi_1)^3}\right)\right].\end{aligned} \tag{12}$$

The stress components demonstrate a strong singularity of the form $1/(x-\xi_2)$. It is also noted that $\sigma_{yy}^{\perp}(x,0;\xi_2)$ contains $D_y^{\perp}$ but not $D_x^{\perp}$, while $\sigma_{xy}^{\perp}(x,0;\xi_2)$ contains $D_x^{\perp}$ but not $D_y^{\perp}$. In other words, the expressions for the normal and shear stresses are decoupled. Also, (11) and (12) are the stress components for an isolated dislocation. For a distribution of dislocations, the dislocation strengths $D_x^{\perp}$ and $D_y^{\perp}$ in (11) and (12) are replaced by the dislocation strength *densities*

$$A_x^{\perp}(\xi_2) = \frac{\partial D_x^{\perp}}{\partial \xi_2}, \qquad A_y^{\perp}(\xi_2) = \frac{\partial D_y^{\perp}}{\partial \xi_2}. \tag{13}$$

The corresponding stresses are then obtained by integrating (11) and (12) with respect to ξ_2 from $\xi_2 = 0$ to $\xi_2 = l$.

In Subproblem 3, the stress field in the cylinder due to a pair of equal and opposite surface line loads P directed along a diameter (the y-axis) is given by Timoshenko and Goodier [13]. In particular, the normal and shear stresses on $y = 0$ are

$$\sigma_{yy}^{p}(x,0) = \frac{P}{\pi R}\left[\frac{4R^4}{(R^2+x^2)^2} - 1\right], \tag{14}$$

$$\sigma_{xy}^{p}(x,0) = 0. \tag{15}$$

The superscript symbol p indicates line loads. Unlike the disclination or the dislocation stresses, these stress components are independent of the elastic constants. Also, the magnitude of the normal stress assumes the maximum value of $3|P|/(\pi R)$ at $x = 0$ and the minimum value of 0 at $x = R$.

2.4. INTEGRAL EQUATIONS

To satisfy (3), the normal and shear stresses at the crack location in the three subproblems are superimposed and set equal to zero, i.e.,

$$\int_0^l \sigma_{yy}^{\perp}(x,0;\xi_2)\,\mathrm{d}\xi_2 + \sigma_{yy}^{\nabla}(x,0) + \sigma_{xy}^{p}(x,0) = 0, \tag{16}$$

$$\int_0^l \sigma_{xy}^{\perp}(x,0;\xi_2)\,\mathrm{d}\xi_2 + \sigma_{xy}^{\nabla}(x,0) + \sigma_{xy}^{p}(x,0) = 0, \tag{17}$$

where $0 \leqslant x \leqslant l$. Equations (16) and (17) are two decoupled Cauchy singular integral equations with the unknown density functions $A_x^{\perp}(\xi_2), A_y^{\perp}(\xi_2)$.

To solve these equations, the method of Gerasoulis [14] is used. His method has been successfully adapted to the solution of singular integral equations which arise in kinked crack problems (see, e.g., Lo [15], He and Hutchinson [16], Niu and Wu [17]). A kinked crack consists of a main crack to which a kink is joined at either crack tip. Computationally, the kinked crack problem and the present problem are similar. In one of the subproblems of the kinked crack problem, the main crack is subjected to the loading of a dislocation distribution which replaces the connecting kink. The stress singularity exponent λ at the kink knee, i.e., where the kink joins the main crack, varies from 0 to 0.5 as the kink angle varies from 0° to 180° (see [16]). In the numerical solutions of the problem, however, $\lambda = 1/2$ is assumed

[15, 16, 17]. This, with an additional condition, leads to correct values of the stress intensity factors and for comparable levels of accuracy requires far less computations than would be needed if the correct value of λ is used [16]. This is because a large number of numerical integrations are needed for an exponent other than 0 or 1/2, while numerical integrations can be avoided for the exponent of 0 or 1/2 due to the availability of the integrals in closed forms. Furthermore, it is shown by Niu and Wu [17] that even when $\lambda = 0$ theoretically, the use of the maximum value $\lambda = 1/2$ yields accurate solutions provided a sufficient number of collocation points is used in the numerical scheme. In the present problem, the disclination defect, which possesses a logarithmic stress singularity, replaces the main crack. The value of λ at the crack head, i.e., where the crack joins the disclination, cannot be determined by the present approach. In view of the above discussion, however, the actual value of λ used in the numerical scheme is not critical, and is taken to be 1/2 in this paper.

The numerical technique can now be summarized as follows. First, (16) and (17) can be normalized to the interval $[-1,1]$ by writing

$$\xi_2 = \frac{l}{2}(1+t), \qquad x = \frac{l}{2}(1+s), \tag{18}$$

where $-1 \leqslant s, t \leqslant 1$. Then, the dislocation strength densities are written as the product of a weight function $w(t)$ and an unknown function $\phi_x(t)$ or $\phi_y(t)$, i.e.,

$$A_x^{\perp}(t) = w(t)\phi_x(t), \qquad A_y^{\perp}(t) = w(t)\phi_y(t), \tag{19}$$

where

$$w(t) = \frac{1}{(1-t)^{1/2}(1+t)^{1/2}}. \tag{20}$$

In (20), the singularity exponents of $w(t)$ at the head of the the crack ($t = -1$) and at the crack tip ($t = 1$) are both assumed to be 1/2. An additional condition $\phi_x(-1) = \phi_y(-1) = 0$ to ensure uniqueness is used in conjunction with this assumption [15, 16]. Also, piecewise quadratic polynomials are used to approximate ϕ_x and ϕ_y [14]. The interval $[-1,1]$ is divided into $2M$ intervals. The use of $2M$ collocation points and the additional condition generates two linear algebraic systems each containing $2M + 1$ equations. The unknowns in the two systems of equations are respectively $\phi_x(t)$ and $\phi_y(t)$ at the boundary points of the $2M$ intervals.

2.5. Stress intensity factors and crack opening displacement

After solving for $\phi_x(t)$ and $\phi_y(t)$, the SIFs can be determined from the limit of the stress field on the x-axis as x approaches the crack tip from outside the crack. Denoting the complex SIF as $K = K_{\mathrm{I}} + iK_{\mathrm{II}}$, where K_{I} and K_{II} are the mode I and mode II SIFs and $i = \sqrt{-1}$, the limit takes the form

$$K = \lim_{x \to l}[\sqrt{2\pi(x-l)} \bullet (\sigma_{yy}^{\mathrm{tot}} + i\sigma_{xy}^{\mathrm{tot}})], \tag{21}$$

where $\sigma_{yy}^{\mathrm{tot}}$ and $\sigma_{xy}^{\mathrm{tot}}$ are the total stress components obtained by superposition. These stresses take exactly the same form as the left sides of (16) and (17). Only the singular terms of the

stresses, however, are of relevance in (21). From (11) and (12), and noting that $A_x^{\perp}(\xi_2), A_y^{\perp}(\xi_2)$ replace $D_x^{\perp}(\xi_2), D_y^{\perp}(\xi_2)$, these singular terms can be written as

$$\sigma_{yy}^{\perp} + i\sigma_{xy}^{\perp} = \int_0^l \frac{A_y^{\perp} + iA_x^{\perp}}{x - \xi_2}\, \mathrm{d}\xi_2. \tag{22}$$

The combination of (21) and (22) leads to the following expression for K

$$K = \lim_{x \to l} \left[\sqrt{2\pi(x-l)} \int_0^l \frac{A_y^{\perp} + iA_x^{\perp}}{x - \xi_2}\, \mathrm{d}\xi_2 \right]. \tag{23}$$

Converting to non-dimensionalized variables using (18), and with substitutions from (19) and (20), (23) can be rewritten as

$$\begin{aligned} K &= \lim_{s \to 1} \left[\sqrt{\pi l(s-1)} \int_{-1}^{1} \frac{\phi_y(t) + i\phi_x(t)}{(s-t)\sqrt{1-t^2}}\, \mathrm{d}t \right] \\ &= \lim_{s \to 1} \left[\sqrt{\pi l(s-1)} \oint_{\Gamma} \frac{\phi_y(t) + i\phi_x(t)}{2(s-t)\sqrt{1-t^2}}\, \mathrm{d}\Gamma \right]. \end{aligned} \tag{24}$$

In (24), Γ is a clockwise contour around the crack and the contour integral can be easily evaluated (see, e.g., Muskhelishvili [18]). Taking the limit, the final result is

$$K = \left(\frac{\pi^3 l}{2} \right)^{1/2} [\phi_y(1) + i\phi_x(1)]. \tag{25}$$

The above solution, although numerically approximate, is obtained from an exact theory. It can also be seen that the computation of K involves the values of $\phi_y(t) + i\phi_x(t)$ at $t = 1$ only. Furthermore, (25) differs from the expression for a kinked crack [15] by a factor of 2 because the dislocation strength density is defined differently for the kinked crack problem.

The approximate expression for computing K can be obtained from the Green's function formula

$$K = \left(\frac{2}{\pi l} \right)^{1/2} \int_0^l (\sigma_{yy} + i\sigma_{xy}) \sqrt{\frac{x}{l-x}}\, \mathrm{d}x, \tag{26}$$

where $(\sigma_{yy} + i\sigma_{xy})$ is the complex stress associated with either the disclination or the line loads or both. In deriving the above formula, the stress redistribution is ignored. Furthermore, the derivation makes use of the Green's function formula for a pair of line loads acting on the crack surface in an *infinite* body. The disclination stress field substituted in the Green's function formula, on the other hand, is derived for a *finite* cylinder.

Consider the SIFs due to the disclination. After substituting the disclination stresses from (5) and (6), (26) becomes

$$\begin{aligned} K &= \left(\frac{2}{\pi l} \right)^{1/2} \int_0^l D^{\nabla} \left(1 + \ln \frac{x}{R} \right) \sqrt{\frac{x}{l-x}}\, \mathrm{d}x \\ &= D^{\nabla} \left(\frac{\pi l}{2} \right)^{1/2} \left[2 + \ln \left(\frac{l}{R} \right) - 2\ln 2 \right]. \end{aligned} \tag{27}$$

Note that K is real in (27), i.e., $K = K_{\mathrm{I}}$ and $K_{\mathrm{II}} = 0$. Also, if K_{I} is divided by $D^{\nabla}\sqrt{l}$ or $D^{\nabla}\sqrt{R}$ and plotted against l/R, a universal curve independent of the elastic constants and the disclination power can be obtained. In passing, it should be mentioned that the crack length in [7] and [10] is estimated by the 'configurational force' method in which a certain mean weighted stress acting on the crack segment is computed. This mean weighted stress takes a similar form to (27). In fact, the configurational force method is equivalent to the method of setting the SIF or the energy release rate to its critical value.

If the disclination is absent and line loads P are applied, K_{II} is also 0 and $K = K_{\mathrm{I}}$ can be evaluated in a similar way, i.e.,

$$K = \left(\frac{2}{\pi l}\right)^{1/2} \int_0^l \frac{P}{\pi R}\left[\frac{4R^4}{(R^2+x^2)^2} - 1\right]\sqrt{\frac{x}{l-x}}\,\mathrm{d}x. \tag{28}$$

A closed-form formula containing the hypergeometric function $F(a, b; c; x)$, in which a, b, c are constants and x is a variable, can be obtained. This can be written as

$$K = \left(\frac{2}{\pi l}\right)^{1/2} P\left(-\frac{5}{4}\frac{l^3}{R^3}F\left(\frac{7}{4}, \frac{9}{4}; \frac{5}{2}; -\frac{l^2}{R^2}\right)\right.$$
$$\left. +2\sqrt{2}\frac{[(l^2/R^2+1)^{1/2}-1]^{1/2}}{(l^2/R^2+1)^{1/2}} - \frac{1}{2}\frac{l}{R}\right). \tag{29}$$

If K_{I} in (29) is divided by $P/\sqrt{l}$ and plotted against l/R, a universal curve independent of P can be obtained. Equations (27) and (29) are added when both the disclination and the line loads are present.

Finally, the crack opening displacement in both the x- and y- directions can be computed from (7), i.e.,

$$[u_x + iu_y] = -\frac{2\pi(1-v)}{\mu}\int_l^x (A_x^{\perp} + iA_y^{\perp})\,\mathrm{d}x, \tag{30}$$

since $A_x^{\perp}$ and $A_y^{\perp}$ are now known at the boundary points of the intervals used in the numerical scheme. Note that (30) is based on the exact theory.

3. Numerical results

All results, unless otherwise stated, are computed from the exact theory. They are grouped in three different sub-sections. Section 3.1 contains an example of a convergence study to determine the number of collocation points necessary to attain convergence of the SIFs. In Section 3.2, the dependence of the $K_{\mathrm{I}} - l/R$ relationship on the disclination power Ω, the structural size R and the line loads P is investigated. In Section 3.3, stable and unstable solutions for the crack length are sought. The dependence of the equilibrium crack length on Ω, R and P is investigated. The SIFs and the crack lengths predicted from the exact and approximate theories are compared in order to quantify the discrepancies between them. In Section 3.4, the opening displacement is investigated, particularly its dependence on Ω, R and P. It should also be mentioned that the mode II SIFs as computed from the exact theory are zero, a result also obtained from the approximate theory.

Table 1. Convergence of the normalized stress intensity factor $\tilde{K}_I = K_I/(|D^\nabla|\sqrt{R})$ at the crack tip due to a negative wedge disclination of strength D^∇ located centrally in a cylinder of radius R. For various ratios of the crack length to structural radius, the solutions improve with the increase in the number of collocation points $2M$.

l/R	$M = 8$	$M = 32$	$M = 64$	$M = 128$	$M = 256$
0.01	1.208	1.221	1.236	1.241	1.244
0.10	2.002	2.042	2.090	2.104	2.114
0.20	2.070	2.127	2.195	2.215	2.229
0.40	1.872	1.952	2.048	2.076	2.096
0.60	1.514	1.612	1.729	1.763	1.787
0.80	0.982	1.095	1.230	1.270	1.297

The elastic constants used are those for aluminum, i.e., $\mu = 26$ GPa and $\nu = 0.347$. Assuming plane strain, the critical stress intensity factor $K_{IC} = 0.361$ MPa $m^{1/2}$ is computed from the grain boundary fracture energy $\gamma_f = 0.818$ Jm^{-2} for aluminum (e.g., Hirth and Lothe [19]) using the formula $K_{IC} = \sqrt{4\gamma_f\mu/(1-\nu)}$. The disclination strength, structural size and line load magnitude considered lie in the range $0° > \Omega > -3°, 0 > l/R > 10^{-8}$ and 5 kN/m $> P > -5$ kN/m, respectively. Structural sizes between 0.5 μm and 100 μm are typical of subgrain and grain sizes in polycrystalline metals, while the larger size of 10 mm corresponds to the scale of a polycrystalline specimen.

3.1. Convergence study

The configuration considered is shown in Figure 1(a) with $P = 0$. The normalized K_I, defined as $\tilde{K}_I = K_I/(|D^\nabla|\sqrt{R})$, is computed for various values of the normalized crack length, i.e., $0.01 \leqslant l/R \leqslant 0.8$. See Table 1. To study convergence, let $2M$ denote the number of collocation points ($8 \leqslant M \leqslant 256$). Define also the percentage difference between the solutions computed with two different values M_c and M_p of M as $\varepsilon = 100\,\% \times [\tilde{K}_I(M_c) - \tilde{K}_I(M_p)]/\tilde{K}_I(M_p)$. Then for the case of $l/R = 0.01$ and (M_p, M_c) equal to (8, 32), (32, 64), (64, 128) and (128, 256), $\varepsilon = 1.08\,\%, 1.23\,\%, 0.40\,\%$ and $0.24\,\%$ correspondingly. For $l/R = 0.8$ and for the same sequence of (M_p, M_c), $\varepsilon = 11.5\,\%, 12.3\,\%, 3.33\,\%$ and $2.13\,\%$. This suggests that the solutions converge more slowly for crack lengths comparable to the structural radius. All the results shown subsequently are generated with $M = 256$.

3.2. Dependence of the SIF on the crack length

In Figure 2, K_I is plotted against $\log_{10}(l/R)$. Figure 2(a) shows how the relation depends on Ω for $R = 50$ μm. Figure 2(b) shows how it depends on R for $\Omega = -1°$. In both Figures 2(a) and (b), $P = 0$. Figure 2(c) shows the dependence on P for $\Omega = -1°$ and $R = 50$ μm. For these cases, K_I initially increases with $\log_{10}(l/R)$ but decreases when $\log_{10}(l/R)$ reaches a value between 0 and -1. For a given l/R, Figure 2(a) shows that increasing the disclination strength increases K_I, as expected, while Figure 2(b) shows that increasing the structural size also increases K_I. In the latter case, this implies that for two geometrically similar cylinders of different sizes (with equal l/R), it is the longer crack in the larger cylinder that has the larger

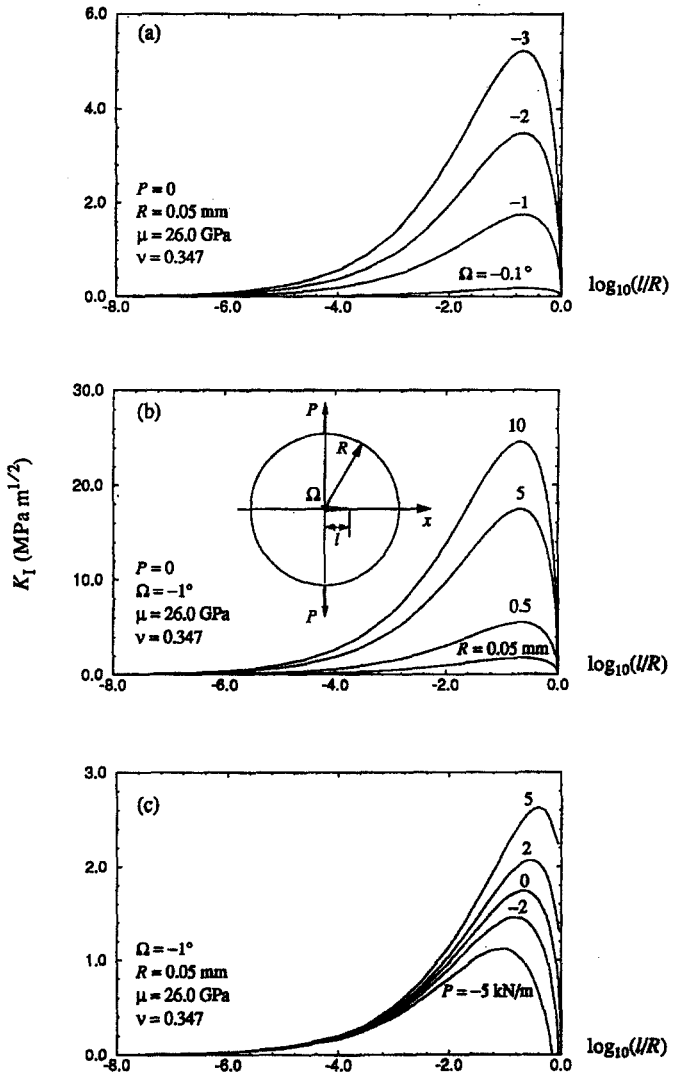

Figure 2. Variations of the mode I stress intensity factor with the normalized crack length. (a) Effect of disclination power. (b) Effect of cylinder radius. (c) Effect of line loads.

K_I. Furthermore, K_I increases with P if P is tensile, but decreases with it if it is compressive. The maxima of the curves occur at increasingly larger values of $\log_{10}(l/R)$ as P changes from compression to tension. The resulting effect is that the curves are skewed towards the larger values of $\log_{10}(l/R)$.

In Figure 3(a), $\tilde{K}_I = K_I/(|D^\nabla|\sqrt{R})$ is plotted against $\log_{10}(l/R)$, while in Figure 3(b) $\tilde{K}_I = K_I/(|D^\nabla|\sqrt{l})$ is plotted against the same parameter. It is assumed that $P = 0$. A universal curve is obtained in each case since each curve is independent of D^∇, l and R. For R fixed at *any* value, Figure 3(a) predicts that K_I increases but subsequently decreases with l. Note that Figure 2(a) makes this assertion only for $R = 50\ \mu$m. The scaling law between K_I and l at fixed R is not obtained in closed form from the exact theory, although the approximate solution (27) suggests a scaling law of the form $(l)^{1/2}$ (constant $-\ln l$). The implication is that the length of a crack growing in the stress field of a disclination is inherently limited by R, i.e.,

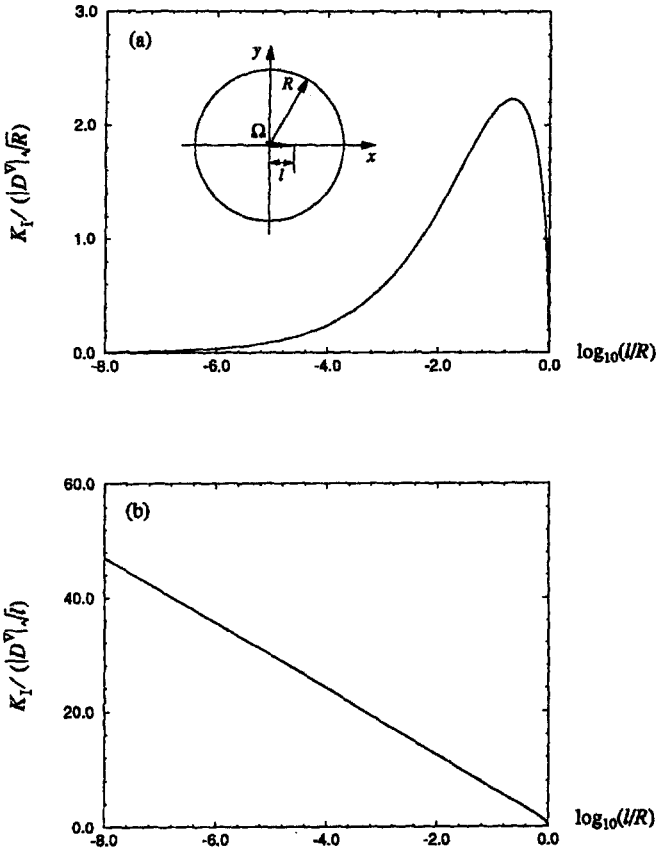

Figure 3. Universal curves of the relation between normalized stress intensity factor and normalized crack length. (a) K_I is normalized by $|D^\nabla|\sqrt{R}$. (b) K_I is normalized by $|D^\nabla|\sqrt{l}$.

the structural or grain size. In contrast, Figure 3(b) predicts that K_I increases monotonically with R for any fixed l. This result is not entirely obvious from Figure 2(b). Also, the scaling law between K_I and R at fixed l is logarithmic according to the approximate theory. It can be inferred that a growing crack nucleus will reach K_{IC} in a large cylinder at a smaller length, implying that a polycrystal with a larger grain size will contain smaller cracks. This prediction is true only for the very short (submicroscopic) cracks. Long (microscopic) cracks with large theoretical K_I values will drop to K_{IC} in a large cylinder at a larger crack length, implying that a polycrystal with a larger grain size will contain longer microscopic cracks. The results of actual computations are shown in Section 3.3.

3.3. Dependence of Equilibrium Crack Length on Ω, R and P

Figure 4(a) shows a plot of K_I versus $\log_{10}(l/R)$ for $\Omega = -1°$, $R = 50$ μm and $P = 0$. The bold and light curves are the solutions of the exact and approximate theories, respectively. It is apparent that K_I obtained from the approximate theory represents a significant underestimate when $\log_{10}(l/R) > -4$. Intuitively, the stress acting on the future crack location unloads once the traction-free crack surfaces are created and redistributes to the crack tip where it is further amplified. Since this is not taken into account in the approximate theory, its prediction

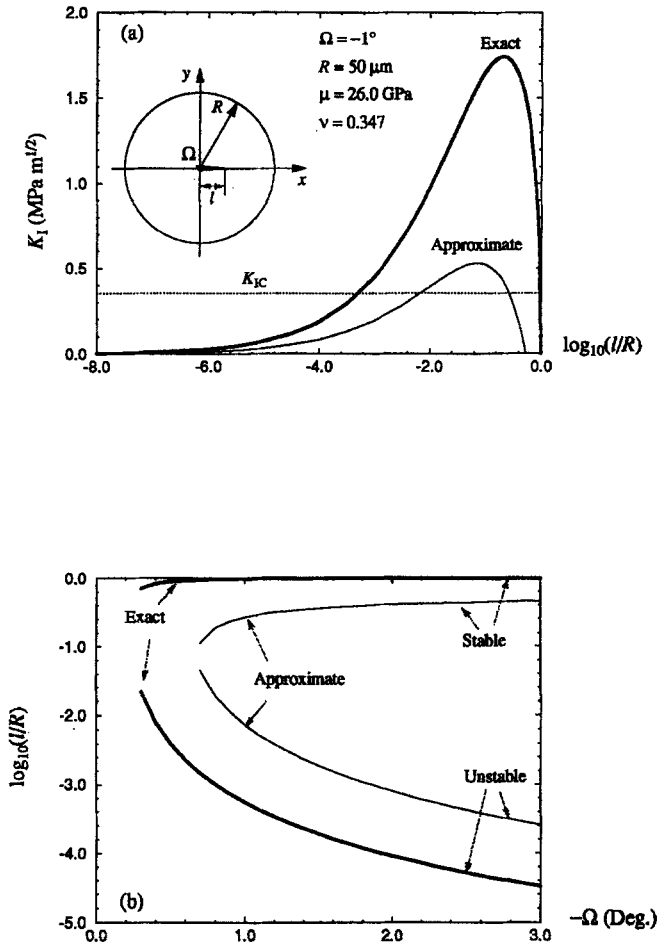

Figure 4. Predictions of (a) the mode I stress intensity factor and (b) the normalized crack length using both the exact and approximate theories. The cylinder radius equals 50 μm and $P = 0$. Significant discrepancies in K_I are predicted for $\log_{10}(l/R) > -4$. Discrepancies in $\log_{10}(l/R)$ between half an order and one order of magnitude are predicted for disclinations with powers between $-0.3°$ and $-3°$. Two families of cracks are predicted – unstable submicroscopic cracks such that $10^{-4.5}R < l < 10^{-1.5}R$, and stable microscopic cracks such that $10^{-0.2}R < l < 10^{0}R$.

is likely to be an underestimate. There is a prevalent assumption that the negligence of stress redistribution in estimating K_I of a wedge crack is acceptable provided that $l/R <\sim 0.15$. This is too unconservative at least for the present case of a disclination defect since the criterion should be $l/R <\sim 10^{-4}$.

The horizontal straight line corresponds to $K_{IC} = 0.361$ MPa m$^{1/2}$. The values of $\log_{10}(l/R)$ read off from the intersections between the horizontal line and the curves give the equilibrium crack lengths. It can be seen that two solutions are predicted. The short crack is unstable since $\partial K_I/\partial(\log_{10}(l/R)) > 0$, while the long crack is stable since $\partial K_I/\partial(\log_{10}(l/R)) < 0$. Both Rybin and Zhukovskii [7] and Gutkin and Ovid'ko [10] gave only the small crack length. They used the approximate theory and did not discuss its stability.

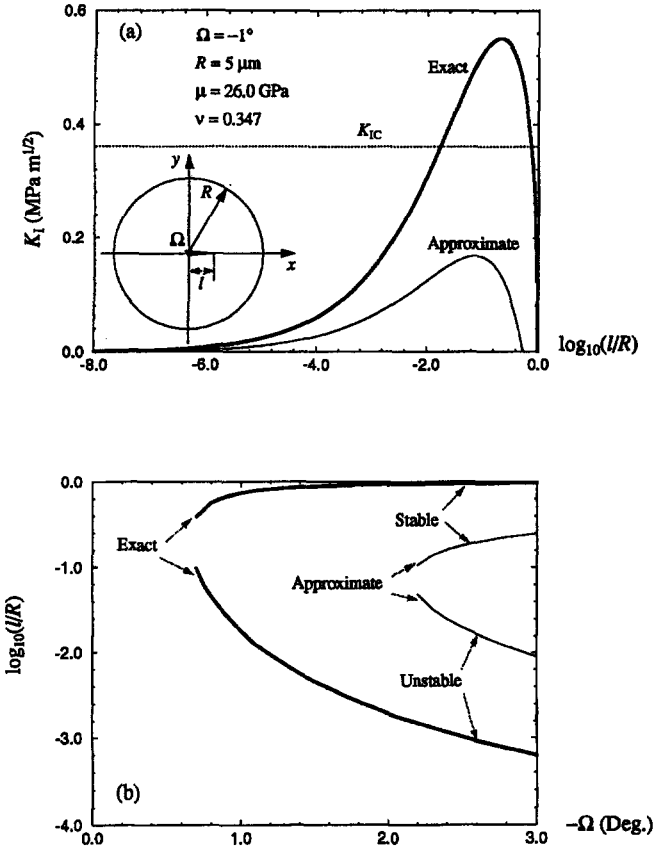

Figure 5. Predictions of (a) the mode I stress intensity factor and (b) the normalized crack length using both the exact and approximate theories. The cylinder radius equals 5 μm and $P = 0$. Significant discrepancies in K_I are predicted for $\log_{10}(l/R) > -4$. DIscrepancies in $\log_{10}(l/R)$ between half an order and one order of magnitude are predicted for disclinations with powers between $-0.7°$ and $-3°$. Two families of cracks are predicted – unstable submicroscopic cracks such that $10^{-3}R < l < 10^{-1}R$, and stable microscopic cracks such that $10^{-0.4}R < l < 10^{0}R$.

For the prescribed value of R, Figure 4(b) compares the crack length predictions of the exact and approximate theories as the disclination strength increases. The approximate theory underestimates the large crack length but overestimates the small crack length. The discrepancies (i) vary between half an order and one order of magnitude, (ii) are larger for the disclinations of smaller powers, and (iii) are larger for the short unstable cracks. The last point requires further emphasis because it is often assumed that the errors of the approximate theory are small when used to compute small crack lengths of the order of a micron, while the errors are large if the predicted crack lengths occupy more than $\sim$ 10 % of the grain boundary length. As far as the order of magnitude is concerned, the present results suggest that the errors of the approximate theory are large for both the small and large crack lengths.

Additional observations of Figure 4(b) can be made. In the case of the exact theory, $\log_{10}(l/R)$ of the short crack decreases from ~ -1.5 to ~ -4.5 as $-\Omega$ increases from 0.3° to 3.0°. On the other hand, $\log_{10}(l/R)$ of the long crack increases from ~ -0.2 to ~ 0 for the same variation of $-\Omega$. Also the lengths of the stable and unstable cracks appear to approach each other as $-\Omega$ decreases below 1°.

The computations of Figure 4 are repeated for a structural size one-tenth smaller, i.e., $R = 5\ \mu$m. The results are shown in Figure 5. Consider the predictions of the exact theory. As $-\Omega$ increases from 0.7° to 3.0°, $\log_{10}(l/R)$ of the short crack now varies from ~ -1 to ~ -3 while $\log_{10}(l/R)$ of the long crack varies from ~ -0.4 to ~ 0. Comparing the results of Figures 4(b) and (5b) and interpreting the structural size to be the grain size, the following observation can be made. For a given Ω and in the case of the short cracks, the crack length to grain size ratio tends to be *smaller* if the grain size is larger. The opposite is true for the long cracks, i.e., the ratio tends to be *larger* if the grain size is larger. A yet stronger observation can be made if actual values form Figure 4(b) and Figure 5(b) are compared, i.e., the above statements remain true if the 'crack length' replaces the 'crack length to grain size ratio'. The results for the short cracks are markedly different from the notion that the crack size scales with the grain size, i.e., l/R is a constant, as is sometimes assumed for a polycrystal subjected to mechanical loading on its external boundary.

Another important observation of Figure 5(a) can be made, i.e., the horizontal K_{IC} line does not intersect the K_I curve constructed from the approximate theory. This suggests that it may not be possible for such a crack to nucleate in the first place. More generally, Figure 5(b) shows that crack nucleation from a disclination may not occur if $-\Omega < 0.6°$ according to the exact theory or if $-\Omega < 2°$ according to the approximate theory.

Figure 6 shows the influence of the compressive loads $P = -5$ kN/m on crack length prediction. All parameters in Figures 4 and 6 are the same except for P. Comparing the two figures, it can be seen that the compressive loads *increase* the size of the short cracks whereas they reduce the size of the long cracks. The change to the crack length introduced by $P \neq 0$, however, is negligible at large $-\Omega$ and moderate for $-\Omega < 1°$. As illustrated in Figure 2(c), changing P from 5 to -5 kN/m suppresses strongly the peak of the K_I versus $\log_{10}(l/R)$ curve but only weakly the tail ends of the curve. This suggests that the application of P does not have great effects on the crack length unless the disclination strength is weak. Although not shown, it may be noted that tensile loads decrease the size of the short cracks whereas they increase the size of the long cracks.

The results in this section suggest that two families of cracks may exist in a polycrystal containing triple line disclinations – the microscopic cracks of the order of the grain size and the submicroscopic cracks approximately 10^{-5} to 10^{-1} times the grain size depending on the geometrical and physical details. Both submicroscopic and microscopic cracks have indeed been reported and emphasized in the experimental observations of aluminum and zinc [9]. The values of $\log_{10}(l/R)$ measured vary between -3 to 0 or greater. In real units, the cracks measure between the extremes of 0.2 μm and 600 μm. Because the submicroscopic cracks nucleated by disclination sources alone are theoretically predicted to be unstable, it is possible that at least some will propagate to reach their stable and longer equilibrium lengths. The approximate analysis of Wu [11] shows that submicroscopic cracks formed by the combined mechanisms of singular disclinations and grain boundary dislocation pile-ups at triple lines are stable. Submicroscopic cracks formed by the single mechanism of grain boundary dislocation pile-ups are also found to be stable by Wu and Zhou [20]. Consequently, the experimentally observed submicroscopic cracks are likely to have been formed under the operation of various pure and mixed mechanisms involving possibly disclinations and grain boundary dislocations.

A final comment is made here regarding the value of R. The equivalence between the grain size and the structural size is almost invariably assumed in dislocation and disclination theories. This appears to yield results consistent with experimental data. Theoretically speaking, however, R should be the specimen size because the normal and shear stresses of the

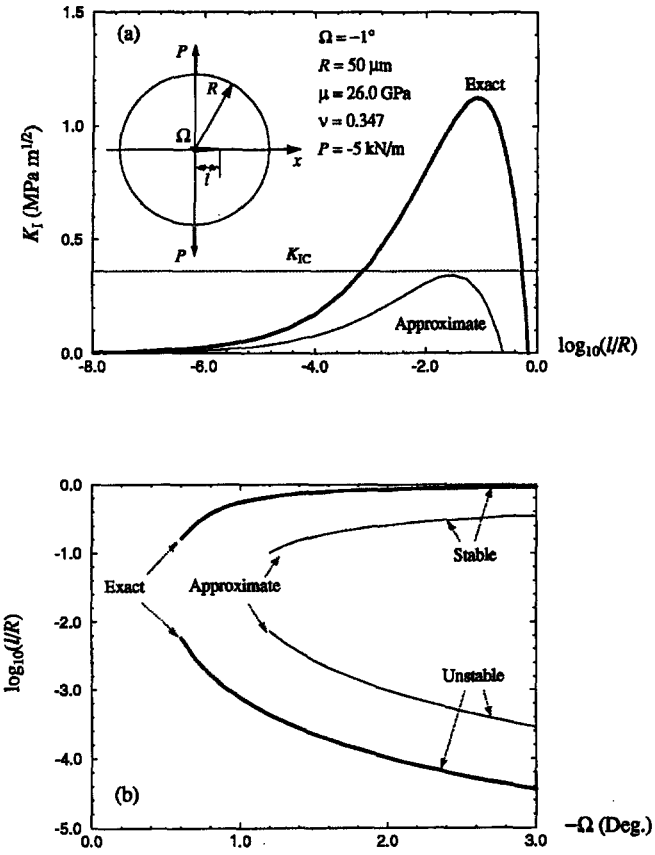

Figure 6. Predictions of (a) the mode I stress intensity factor and (b) the normalized crack length using both the exact and approximate theories. The cylinder radius equals 50 μm and $P = -5$ kN/m. Comparing Figures 4 and 6, the influence of P on the crack length is moderate for disclination powers $(-\Omega)$ less than about a degree and is negligible for larger disclination powers.

disclination does not in reality vanish on the exterior of the grain size region containing the disclination. The specimen surface, in contrast, is traction-free if the loading arises entirely from internal sources. Yet if R is chosen to be the specimen size, e.g., $R = 5$ mm, the two values of $\log_{10}(l/R)$ predicted using Figure 2(b) are approximately -6 and 0, corresponding to the actual sizes of 0.005 μm and 5 mm. For this example and others, the short crack appears to be very small while the long crack essentially spans the entire specimen. These predictions, possibly incorrect, have at least two causes. First, the stress field derived for a singular disclination simply ceases to be valid outside the grain size region because of the presence of multiple defects of the same type or of other types, or because of the interference of the stress fields by inhomogeneities on the scale of the grains. Second, if the long cracks are approaching the specimen size, then the use of a microscopic fracture toughness derived from the grain boundary fracture energy may not be valid. The long cracks may not be straight as assumed and must span many grain diameters.

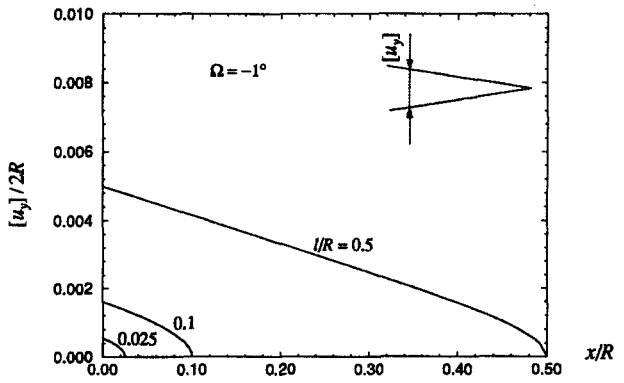

Figure 7. The normalized opening displacement (divided by 2) for various crack length to cylinder radius ratios. The disclination power Ω equals $-1°$. The opening displacement is independent of the elastic constants. The crack profile is wedge-shaped.

3.4. Opening displacement

The opening displacement in the x-direction, $[u_x]$, is found to be zero. The opening displacement $[u_y]$ divided by 2 can be normalized by R and plotted against the normalized x-coordinate, x/R. Figure 7 shows such a plot for $\Omega = -1°$ and $P = 0$. The three curves correspond to the crack lengths $0.025R, 0.1R$ and $0.5R$, respectively. The maximum opening displacements corresponding to these three crack lengths are $\sim 0.001R, 0.0032R$ and $0.01R$. The aspect ratio $[u_y]/l$ decreases as l increases, i.e., the crack profile becomes flatter as the crack increases in length. It can also be seen that the predicted crack profiles are wedged-shaped.

It is found that the curves, normalized or not, are independent of the elastic constants μ and ν. This can be rationalized by noting that although a crack in a stiff material with a large μ tends to open less, a large μ is also associated with a larger disclination stress field. This stress field tends to wedge open the crack with greater intensity and compensates for the reduced opening associated with the stiff material. The opening displacement is, however, dependent on Ω because Ω changes the stress field but not the stiffness of the material. Moreover, the normalized curves are found to be independent of R.

Finally, Figure 8 examines the effect of P on the opening displacement for the case of $l = 0.5R$ and $\Omega = -1°$. In this figure, $R = 50$ μm. Because Ω and P have different effects on the relation between $[u_y]$ and R, these normalized curves, except for $P = 0$, are dependent on R. As expected, tensile loads increase the opening, while compressive loads reduce the opening. It is interesting to observe the change of the crack profile from convex upward to convex downward (except in the vicinity of the crack tip) as the line loads change from tensile to compressive.

4. Conclusions

An exact theoretical formulation for a crack in a disclinated cylinder is provided in this paper. The disclination is of the negative wedge type, and its axis coincides with the long axis of the cylinder. The head of the crack is at the location of the disclination. The cylinder may also be subjected to equal and opposite line loads perpendicular to the crack and passing through the

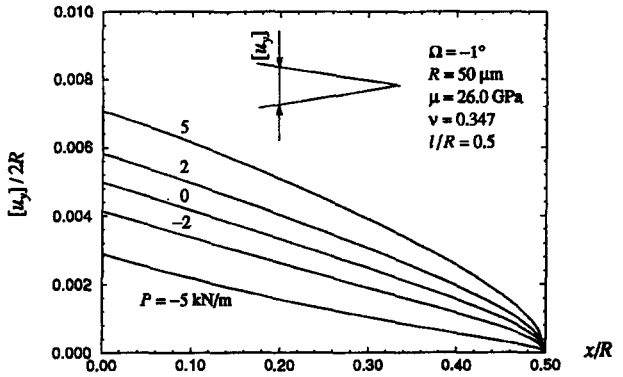

Figure 8. The dependence of the crack opening displacement on the surface line loads P. Compressive loads cause a slight deflation of the wedge profile.

center of the circular cross-section. This configuration is an approximate model for triple line disclinations in polycrystalline materials.

The analytical method makes use of superposition in which the original problem is decomposed into subproblems with known solutions for the stress fields. Furthermore, the crack is replaced by a continuous distribution of edge dislocations. Satisfaction of the traction-free condition on the crack results in two decoupled singular integral equations which are solved numerically. Formulas for the stress intensity factor and the opening displacement are derived. Stress intensity factor formulas derived from the approximate theory, which ignores stress redistribution, are also provided.

The relevant parameters of the problem are: disclination power Ω, line loads P, elastic constants μ and ν, structural size R and crack length l. The numerical results show that:

(i) For a given R the scaling law between K_{I} and l is non-monotonic: K_{I} increases with l but subsequently decreases with l when l is between 0.1 R and R. For a given l the scaling law between K_{I} and R is monotonic: K_{I} increases with R.

(ii) The stress intensity factor K_{I} increases with $-\Omega$. Also, K_{I} increases with P if P is tensile, but decreases with it if it is compressive.

(iii) The exact theory predicts unstable submicroscopic cracks 10^{-5} to 10^{-1} times the grain size and stable microscopic cracks of the order of the grain size. If the disclination power is small, the disclination may not be able to nucleate a crack.

(iv) Significant differences exist in the predictions of the exact and approximate theories. Good agreement for K_{I} occurs only for crack lengths below $10^{-4}R$. For $0° < -\Omega < 3°$, discrepancies as large as half to one order of magnitude occur in the crack length predictions. In particular, the discrepancies in the small crack length are even larger than the discrepancies in the larger crack length. These results challenge the previous assumption that the approximate theory is acceptable provided the crack lengths are small, e.g., not greater than $\sim 10^{-1}R$, or ~ 10 μm for $R = 100$ μm.

(v) As the disclination strength increases, the submicroscopic cracks decrease in length while the microscopic cracks increase in length.

(vi) The submicroscopic crack length to grain size ratio decreases as the grain size increases. The microscopic crack length to grain size ratio increases as the grain size increases.

(vii) The application of compressive surface line loads increase the submicroscopic crack lengths but decrease the microscopic crack lengths. The opposite effect occurs if the line loads are tensile.

(viii) The opening displacement $[u_y]$ is independent of the elastic constants. It is however, a function of Ω, P and R. The crack profile is wedge-shaped. A compressive P causes a deflation of the wedge shape. For a crack of half the structural size, the maximum opening displacement, which occurs at the crack head, is $\sim 0.01R$ when $P = 0$.

Acknowledgments

The authors gratefully acknowledge tha financial support of the National Science Foundation (Grant No. CMS-9523028). Partial support also comes from the Center for Materials Research and Analysis, University of Nebraska-Lincoln.

References

1. W. Bollman, Triple lines in polycrystalline aggregates as disclinations. *Philosophical Magazine A* 49 (1984) 73–79.
2. W. Bollman, Triple-line disclinations: representations, continuity and reactions. *Philosophical Magazine A* 57 (1988) 637–649.
3. A.E. Romanov and V.I. Vladimirov, Disclinations in crystalline solids, in *Dislocations in Solids*, Vol. 9, Nabarro, F.R.N. (ed.), Elsevier Science Publishers, Amsterdam, (1992) 191–402.
4. A. Yu Belov, Scaling regimes and anomalies of wedge crack disclination stresses in anisotropic rotationally inhomogeneous media. *Philosophical Magazine A* 68 (1993) 1215–1231.
5. A.A. Nazarov, A.E. Romanov and R.Z. Valiev, On the structure, stress fields and energy of nonequilibrium grain boundaries. *Acta Metallurgica et Materialia* 41 (1993) 1033–1040.
6. A.A. Nazarov, On the role of non-equilibrium grain-boundary structure in the yield and flow stress of polycrystals. *Philosophical Magazine A* 69 (1994) 327–340.
7. V.V. Rybin and I.M. Zhukovskii, Disclination mechanism of microcrack formation. *Soviet Physics, Solid State* 20 (1978) 1056–1059.
8. R.L. Lyles and H.G.F. Wilsdorf, Microcrack nucleation and fracture in silver crystals. *Acta Metallurgica* 23 (1975) 269–277.
9. V.R. Regel, A.M. Leksovskii and S.N. Sakiev, The kinetics of the thermofluctuation induced micro- and macrocrack growth in plastic metals. *International Journal of Fracture* 11 (1975) 841–850.
10. M. Yu Gutkin and I.A. Ovid'ko, Disclinations, amorphization and microcrack generation at grain boundary junctions in polycrystalline solids. *Philosophical Magazine A* 70 (1994) 561–575.
11. M.S. Wu, Crack nucleation due to dislocation pile-ups at I-, U- and amorphized triple lines, accepted for publication in *Mechanics of Materials*, 31p manuscript.
12. J.D. Eshelby, Boundary problems, in *Dislocations in Solids*, Vol. 1, Nabarro, F.R.N. (ed.), North-Holland, Amsterdam, 169–221.
13. S.P. Timoshenko and J.N. Goodier, *Theory of Elasticity*, Third Edition, McGraw-Hill, New York, 567p.
14. A. Gerasoulis, The use of piecewise quadratic polynomials for the solutions of singular integral equations of Cauchy type. *Computers and Mathematics with Applications* 8 (1982) 15–22.
15. K.K. Lo, Analysis of branched cracks. *Journal of Applied Mechanics* 45 (1978) 797–802.
16. M.Y. He and J.W. Hutchinson, Kinking of a crack out of an interface. *Journal of Applied Mechanics* 56 (1989) 270–278.
17. J. Niu and M.S. Wu, Strong interactions of morphologically complex cracks, accepted for publication in *Engineering Fracture Mechanics*, 42p manuscript.
18. N.I. Muskhelishvili, *Some Basic Problems of the Mathematical Theory of Elasticity*, Noordhoff, Leyden, (1977) 732 p.
19. J.P. Hirth and J. Lothe, *Theory of Dislocations*, Second Edition, John Wiley and Sons, New York, (1982) 857 p.
20. M.S. Wu and H. Zhou, An energy analysis of triple junction crack nucleation due to the wedging action of grain boundary dislocations, *International Journal of Fracture* 78 (1996) 165–191.